IOPscience iopscience.iop.org

Home Search Collections Journals About Contact us My IOPscience

Electrowetting-controlled droplet generation in a microfluidic flow-focusing device

This article has been downloaded from IOPscience. Please scroll down to see the full text article.

2007 J. Phys.: Condens. Matter 19 462101

(http://iopscience.iop.org/0953-8984/19/46/462101)

View the table of contents for this issue, or go to the journal homepage for more

Download details:
IP Address: 129.252.86.83
The article was downloaded on 29/05/2010 at 06:41

Please note that terms and conditions apply.

IOP FTC

IOP PUBLISHING JOURNAL OF PHYSICS: CONDENSED MATTER

J. Phys.: Condens. Matter **19** (2007) 462101 (7pp) doi:10.1088/0953-8984/19/46/462101

FAST TRACK COMMUNICATION

Electrowetting-controlled droplet generation in a microfluidic flow-focusing device

Florent Malloggi, Siva A Vanapalli, Hao Gu, Dirk van den Ende and Frieder Mugele

Physics of Complex Fluids, Faculty of Science and Technology, IMPACT and MESA+ Institute, University of Twente, PO Box 217, 7500AE Enschede, The Netherlands

Received 29 August 2007
Published 19 October 2007
Online at stacks.iop.org/JPhysCM/19/462101

Abstract

We studied the generation of aqueous microdrops in an oil–water flow-focusing device with integrated insulator-covered electrodes that allow for continuous tuning of the water wettability by means of electrowetting. Depending on the oil and water inlet pressures three different operating conditions were identified that shift upon applying a voltage: stable oil–water interface, drop generation, and laminar water jet formation. Full control over the drop generation is achieved within a well-defined range of inlet pressures, in quantitative agreement with a model based on the additive contributions from electrowetting and the local hydrostatic pressure at the junction. The tuning power of electrowetting is shown to increase upon device miniaturization, which makes this approach particularly attractive for flow control on the sub-micrometer scale.

(Some figures in this article are in colour only in the electronic version)

The recent upsurge in droplet-based microfluidic research is fueled by the potential application of drops as well-controlled environments for biochemical reactions [1], material synthesis [2–4], single-cell analysis [5, 6], as well as novel fluid logical devices [7]. Commonly pressure-driven flows are used to create droplets continuously either in a flow-focusing [8, 9] or in a T-junction [10] geometry. While this approach provides high throughput capability, it is amenable neither to detailed on-demand generation of individual drops nor to dynamic control of surface wettability, which can dramatically affect the dynamics of two-phase microflows [11, 12]. Alternatively, the electrowetting (EW)-on-dielectric approach is used to digitally manipulate drops [13–15]. Compared to the continuous flow approach, EW provides exquisite control over individual drops and surface wettability. However, current implementations have low throughput and cannot readily be integrated with existing channel-based technologies.

In this letter, we adopt a unified approach to create a soft microfluidic platform that harvests the power of both methods and offers the capability of addressing their limitations. We achieve

 © 2007 IOP Publishing Ltd Printed in the UK

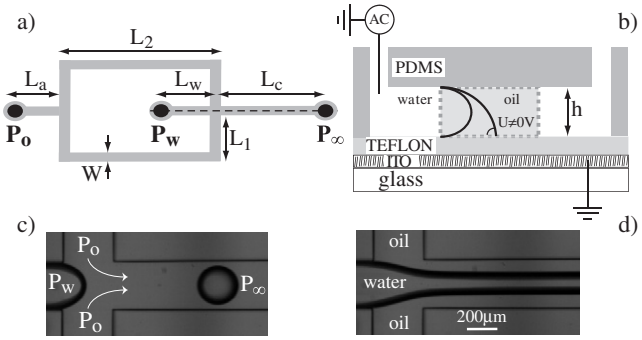

Figure 1. (a) Schematics of the electrowetting-based flow-focusing device (EW-based FFD)—geometry and channels' dimensions: width ($W = 390\ \mu$m), height h and lengths (L_a, $L_0 = L_1 + L_2$, L_w, L_c). (b) Cross-section along the dotted line (see (a)). ((c), (d)) Top views in the drop generation and laminar jetting regime, respectively.

this integration by incorporating EW into a flow-focusing device (FFD) and demonstrate electrowetting-controlled drop formation. We identify experimentally the range of voltages and driving pressures that yields EW-induced droplet generation. A theoretical description based on the balance of external pressures and voltage-controlled capillary pressures quantitatively accounts for the observations. Moreover we show that this unification yields a synergistic outcome: the smaller the geometric scales the more efficient the electrowetting control of drop generation.

Figures 1(a) and (b) illustrate the geometry of the EW-based FFD. The device was made in polydimethylsiloxane (PDMS) using soft lithography [16]. The PDMS structure was clamped mechanically onto an indium tin oxide (ITO)-covered glass substrate, which was pre-coated with a hydrophobic dielectric layer of Teflon AF (thickness $d \approx 4\ \mu$m) following [17]. The elastic nature of PDMS enabled a conformal seal with the bottom electrode. A thin wire immersed into the aqueous phase was used to apply an AC voltage (10 kHz) of 0–170 V_{rms} (root mean square). The fluid flow at the water (deionized water + NaCl with a conductivity $\sigma = 10$ mS cm^{-1}) and oil (mineral oil $\mu_o = 0.03$ Pa s, $\rho_o = 875$ kg m^{-3}) inlets was driven using hydrostatic heads with a precision of 1 Pa ($\equiv$0.1 mm). Young's contact angles measured through the water phase on the top (PDMS) and bottom (Teflon AF) surfaces are $\theta_{top} = 150°$ and $\theta_{bot} = 169°$, respectively. An oil–water interfacial tension of $\gamma = 38$ mN m^{-1} was measured using the pendant-drop method.

To explore the effect of EW on the operation of the FFD, we varied systematically the three control parameters, namely, the inlet water pressure (P_w), inlet oil pressure (P_o) and the voltage (U). Figure 2 reports the resulting phase diagram, which was generated as follows: at zero voltage and constant P_o, the water pressure was increased such that a stable oil–water interface formed at the cross-junction. Upon increasing P_w beyond a critical value P_w^*, this interface becomes unstable and drops are being generated (figure 1(c)) at a constant rate that depends on the absolute values of both P_o and P_w. Upon decreasing P_w again below the critical value, the drop generation ceases immediately without any noticeable hysteresis. Repeating these measurements for various values of P_o, we obtain a linear onset curve $P_w^*(P_o)$ for the generation of drops (filled squares and full line in figure 2). The same experiment was then repeated for a series of applied voltages up to $U_{max} = 150$ V (the maximum voltage is determined by the onset of a contact line instability due to the high local electric fields occurring at $U_c \approx 170$ V in the present device [18]). Again, the critical water pressure turned out to increase linearly

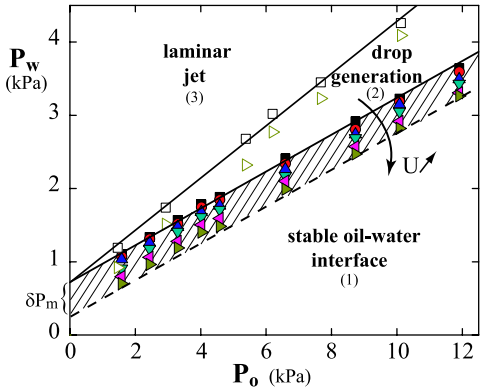

Figure 2. Phase diagram identifying the regime of droplet formation in EW-based FFD ($h = 190\ \mu$m, $W = 390\ \mu$m, $\mu_o/\mu_w = 30$—voltage: ■—□ 0 V, ● 50 V, ▲ 80 V, ▼ 100 V, ◀ 120 V, ▶—▷ 150 V). Hatched area: EW-tuning window with width $\delta P_m = P_L(0) - P_L(U_{max})$.

with P_o—with exactly the same slope λ ($= 0.25 \pm 0.01$ for the present device) as in the purely hydrodynamic case. Denoting the voltage-dependent critical water pressure at $P_o = 0$ as $P_L(U)$, we thus find a family of onset curves described by

$$P_w^*(U, P_o) = P_L(U) + \lambda P_o. \tag{1}$$

This family of curves thus defines an EW-tuning window (hatched in figure 2), in which the generation of drops can be triggered by applying a voltage (while the oil–water interface is stable at zero voltage).

Upon increasing P_w to values beyond P_w^*, we observe variations in the size and frequency of the drops generated and eventually another critical value is reached, above which the drop generation ceases and stable laminar jets are generated, as shown in figure 1(d). Like the onset curve, the resulting upper boundary of the drop generation region (open symbols in figure 2) increased linearly with P_o and shifted downwards upon applying a voltage. Both boundaries extrapolate to the same intercept $P_L(U)$ at $P_o = 0$. In contrast to the onset curves, the transition to the laminar jet displays a substantial hysteresis. In the following, we focus only on the onset curve.

To model the behavior of the onset curves, we have to understand both the observed decrease of $P_L(U)$ with increasing U and the value of the voltage-independent coefficient λ. Since both the typical Reynolds number $Re = \rho L v/\mu \approx 10^{-1}$ and the capillary number $Ca = \mu v/\gamma \approx 10^{-2}$ are small compared to unity, we expect the balance of static pressures to control the system. (v is the characteristic velocity of the mean flow in the outlet channel.) This expectation is corroborated by the fact that the water–oil interface close to drop generation onset appears circular from above, as in static equilibrium (see figure 1(c)). Hence, the idea of our model is the following: to generate drops at the FFD junction, P_w obviously needs to exceed the sum of both the maximum Laplace pressure $P_L(U)$ that the oil–water interface can sustain and the local hydrostatic pressure P_j at the junction. The former is determined by the junction geometry and the voltage-dependent contact angle. The latter is given in analogy to Ohm's law by P_o times a prefactor, λ, that depends on the hydrodynamic resistances of the various channel segments.

Let us consider first the Laplace pressure, which is given by $P_L = \gamma(1/R_w + 1/R_h)$. R_w and R_h are the radii of curvature in the horizontal plane (corresponding to the channel

width W) and in the vertical plane (channel height h) (see figures 1(b) and (c))[1]. Upon drop generation, the three-phase contact line is pinned along the vertical corners on the left side of the junction. Therefore, R_w can adjust itself freely to meet the imposed pressure boundary conditions. Its minimum value is $R_w \approx W/2$, corresponding to the maximum Laplace pressure that the interface can sustain. On the top and bottom surfaces, however, the contact line is free to move. Hence, R_h is determined by the corresponding contact angles and by the channel height. While θ_{top} is constant, the contact angle on the bottom surface, $\theta(\eta)$, decreases with increasing voltage following the well-known electrowetting equation [13]

$$\cos\theta(\eta) = \cos\theta_{bot} + \eta. \tag{2}$$

Here $\eta = \epsilon_0\epsilon_r U^2/2d\gamma$ is the dimensionless electrowetting number, which measures the relative strength of electrostatic and surface tension forces. ϵ_0 and ϵ_r (=2) are the vacuum susceptibility and the dielectric constant. For the present device, the minimum contact angle at $\eta_{max} = \eta(U_{max})$ is $\theta_{min} = 80°$. Under these conditions, the radius of curvature, R_h, depends on the applied voltage and therefore the pressure associated with this interface can be rewritten as

$$P_L(U) = \gamma\left(\frac{2}{W} + \frac{1}{R_h(U)}\right) \tag{3}$$

where the geometric construction sketched in the inset of figure 3(a) relates $R_h(U)$ to the two contact angles:

$$\frac{1}{R_h(U)} = -\frac{2}{h}\cos\left(\frac{\theta(U) - \theta_{top}}{2}\right)\cos\left(\frac{\theta(U) + \theta_{top}}{2}\right). \tag{4}$$

Equations (2)–(4) together establish a quantitative link between the intercept $P_L(U)$ and the applied voltage U. To test this model we extracted $P_L(U)$ by extrapolating the onset curves in figure 2 to $P_o = 0$. The result is plotted in figure 3(a) (▼ and —) in dimensionless coordinates. Excellent agreement between the model and the experimental data is achieved without any fitting parameter. These measurements were further confirmed by measuring directly the water pressure $P_L(U)$ required to bring the oil–water interface to the junction at zero oil pressure in devices with two different channel heights, $h = 190\ \mu$m (●) and 115 μm (□).

Let us now determine the coefficient λ. Considering the equivalent hydrodynamic circuit of the FFD [19] (cf the inset of figure 3(b)) and applying Ohm's law, we find that the local hydrostatic pressure at the junction is given by

$$P_j = \Omega_c/(\Omega_a + \Omega_o/2 + \Omega_c)P_o. \tag{5}$$

Here, Ω ($\approx\mu L/Wh^3$, where μ is the viscosity of the fluid in the corresponding channel segment of length L) denotes the fluidic resistance and subscripts refer to the respective channel segments as shown in the inset of figure 3(b). Note that for channels with uniform cross-sectional area throughout the device, λ depends solely on the length of the various channel segments. Inserting the values for the various Ωs for the data from figure 2, we find $\lambda = 0.26$ in excellent agreement with the experimentally determined value. This result was confirmed for several other channel geometries and liquid combinations, as shown in the inset table of figure 3(b).

The drop generation is thus governed by the very simple criterion that the applied water pressure has to exceed the sum of the local hydrostatic pressure and the Laplace pressure. What does this suggest about the physics involved in the onset of drop formation? What conclusions can be drawn for applications of the method? First, we note that the success of the purely static model corroborates our earlier assumption that hydrodynamic effects arising from both inertial

[1] Strictly speaking, we should determine R_w in the plane containing the surface normal whenever $\theta_{top} \neq \theta_{bot}$. However, this effect turns out to be negligible.

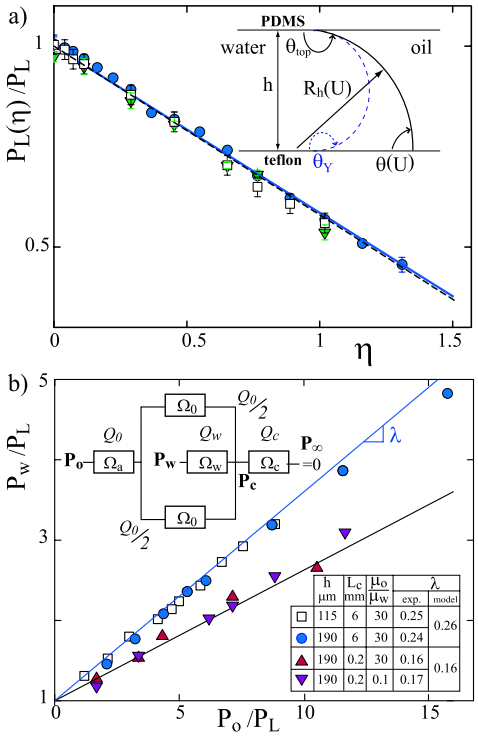

Figure 3. Comparison of experiment and model for the drop onset curve. (a) Normalized pressure $P_L(U)/P_L$ versus electrowetting number η. Symbols: experiments (□ = 115 μm, ●— ▼ = 190 μm); lines: model (190 μm —, 115 μm – – –). Inset: cross-sectional sketch of the interface inside the channel: without EW (– – –), with EW (——). (b) Normalized critical water pressure versus normalized oil pressure for various configurations. Inset: hydrodynamic circuit of the device (top) and table (bottom) showing λ for various device geometries.

and local viscous forces can indeed be neglected. In fact, we can verify explicitly that both contributions are small by analyzing the momentum balance and the viscous stresses due to the flow along the outlet channel. The momentum flux density in the outlet channel is given by $p_{\text{inert}} \approx \rho_o v^2 \approx 0.1$ Pa for a typical velocity $v = \text{O}(1\ \text{cm s}^{-1})$. The viscous normal stress at the oil–water interface is given by $p_{\text{visc}} \approx \mu v/W \approx 1$ Pa, where we assume that the velocity v decays over a typical distance of order W. Hence, both contributions are indeed significantly smaller than typical value of $P_w^*(U)$, which is of order kPa. Note that this is only true at the onset of drop formation. The actual formation processes including the pinch-off *are* affected by viscous forces. Second, $P_L(U)$ and λ, the two parameters that govern the drop generation, can be varied independently by adapting the device geometry to optimize the control that can be achieved by electrowetting. To maximize the influence of EW with respect to the local hydrostatic pressure, one has to minimize λ (cf equation (5)). This is most easily achieved by using a short and/or wide outlet channel with a low resistance Ω_c, as for instance in [9]. Finally, the strength of the electrowetting effect itself can also be tuned by varying the channel height: owing to the $1/h$ scaling of the Laplace pressure (equations (3) and (4)), the tuning range of electrowetting is predicted to increase with decreasing device dimension. As a consequence, the width of the EW-tuning window (cf figure 2) should increase allowing for greater flexibility and wider range of drop-on-demand control.

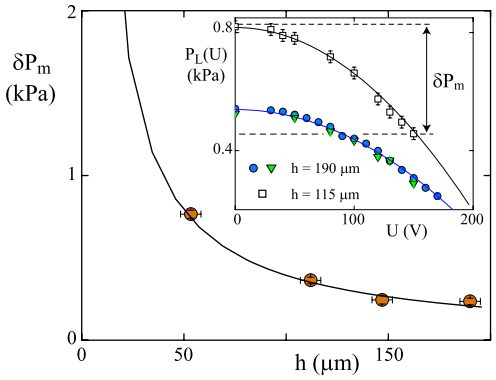

Figure 4. Evolution of δP_m with the channel height h (model ——; experiment ●). Inset: data from figure 3(a) plotted in absolute units. The region delimited by δP_m is the EW-drop generation region. $W = 390\ \mu$m for all geometries.

To verify the latter prediction we measured $P_L(U)$ for four different channel heights, $h = 55$, 115, 160 and 190 μm. In the inset of figure 4, we show the decrease of $P_L(U)$ for two different channel heights on an absolute linear scale. From these data we determined the EW-controlled pressure tuning range $\delta P_m = P_L(0) - P_L(U_{max})$, which is shown in the main panel of figure 4 for the four values of h investigated—in perfect agreement with the model calculation based on equations (2)–(4).

This scaling makes electrowetting a promising tool for the generation of micrometer-sized and even smaller drops. For a characteristic size of 1 μm the corresponding pressure scale is 10^5 Pa. For the present contact angle tuning range, this pressure can be reduced by approximately 50% at $U = U_{max}$. This range can be expanded even more if a second electrode is embedded into the top wall of the channel. In that case, the net curvature of the oil–water interface could be reduced to negative values allowing for drop generation even for situations with $P_w < P_j$. How far can the miniaturization of such a device be extended? The electrowetting equation (equation (2)) assumes implicitly that the thickness of the insulating layer is small. Current technologies allow for insulator thicknesses down to $\lesssim$100 nm (see [13]), indicating that the model developed above should work down to the sub-micrometer range. Even at smaller scales, electrowetting will still promote drop generation; however, then a correct estimate of its strength requires an analysis of the local electric fields and the corresponding Maxwell stresses [20].

In summary, we showed that integrating EW into a microfluidic FFD allows indeed for a detailed electrical control of drop generation. The origin of the observed drop generation threshold is shown to be due to additive contributions from electrowetting and the local hydrostatic pressure at the junction of the FFD. The experimental phase diagram and the concomitant model offer a guide for expanding the capabilities of the EW-based FFD. In particular, we demonstrated that the influence of EW as a control parameter increases upon downscaling, thereby making EW a promising tool also for sub-micrometer-sized devices. We anticipate that the flexibility demonstrated here could be enhanced even further by using specifically patterned electrodes in the junction area and optimized waveforms applied to actuate them. These capabilities allow unprecedented control over drop size and frequency, thus opening up new opportunities for automated drop generation and handling in applications ranging from drop-based synthesis and analysis to emulsification to drop-based logical circuits.

We acknowledge D Wijnperle for assistance with fabrication of devices. We acknowledge MicroNed, the Microtechnology Research Programme of The Netherlands, for financial support, as well as the research institutes IMPACT and MESA+ at Twente University.

References

[1] Song H, Chen D L and Ismagilov R F 2006 *Angew. Chem. Int. Edn* **45** 7336
[2] Xu S, Nie Z, Seo M, Lewis P, Kumacheva E, Stone H A, Garstecki P, Weibel D B, Gitlin I and Whitesides G M 2005 *Angew. Chem. Int. Edn* **44** 724
[3] Fernandez-Nieves A, Cristobal G, Garces-Chavez V, Spalding G C, Dholakia K and Weitz D A 2005 *Adv. Mater.* **6** 680
[4] Nie Z H, Xu S Q, Seo M, Lewis P C and Kumacheva E 2005 *J. Am. Chem. Soc.* **127** 8058
[5] He M Y, Edgar J S, Jeffries G D M, Lorenz R M, Shelby J P and Chiu D T 2005 *Anal. Chem.* **77** 1539
[6] Tan Y-C, Hettiarachchi K, Siu M, Pan Y-R and Lee A P 2006 *J. Am. Chem. Soc.* **128** 5656
[7] Garstecki P, Fuerstman M J and Whitesides G M 2005 *Nat. Phys.* **1** 168
Prakash M and Gershenfeld N 2007 *Science* **315** 832
Fuerstman M J, Garstecki P and Whitesides G M 2007 *Science* **315** 828
[8] Garstecki P, Stone H A and Whitesides G M 2005 *Phys. Rev. Lett.* **94** 164501
[9] Anna S L, Bontoux N and Stone H A 2003 *Appl. Phys. Lett.* **82** 364
[10] Thorsen T, Roberts R W, Arnold F H and Quake S R 2001 *Phys. Rev. Lett.* **86** 4163
[11] Engl W, Ohata K, Guillot P, Colin A and Panizza P 2006 *Phys. Rev. Lett.* **96** 134505
[12] Dreyfus R, Tabeling P and Willaime H 2003 *Phys. Rev. Lett.* **90** 144505
[13] Mugele F and Baret J C 2005 *J. Phys.: Condens. Matter* **17** R705
[14] Cho S K, Moon H J and Kim C J 2003 *Microelectromech. Syst.* **12** 70
[15] Pollack M G, Fair R B and Shenderov A D 2000 *Appl. Phys. Lett.* **77** 1725
[16] Duffy D C, McDonald J C, Schueller O J A and Whitesides G M 1998 *Anal. Chem.* **70** 4974
[17] Seyrat E and Hayes R A 2001 *J. Appl. Phys.* **90** 1383
[18] Vallet M, Vallade M and Berge B 1999 *Eur. Phys. J.* B **1** 583
[19] Knight J B, Vishwanath A, Brody J P and Austin R H 1998 *Phys. Rev. Lett.* **80** 173863
[20] Buehrle J, Herminghaus S and Mugele F 2003 *Phys. Rev. Lett.* **91** 086101